Electronic Supporting Information

Photochemically Induced Self-Healing in a Cadmium(II) Coordination Crystal

Victoria N.P. Pham-Tran, Tristan J. L. LaCasse, Peter Gordon, Katherine M. Marczenko*[a]

[a]Department of Chemistry, Carleton University, Ottawa, ON, Canada

Email: katherinemarczenko@cunet.carleton.ca

Contents

1 General

Synthetic Procedures

Manipulations were performed in air under standard atmospheric conditions. All deuterated solvents were dried and stored over activated molecular sieves (3 Å).

Solution NMR Spectroscopy

All Nuclear Magnetic Resonance (NMR) experiments were carried out on a Bruker AV-300 spectrometer in dried deuterated solvent. Residual ^{1}H signal of the deuterated solvent was used for chemical shift calibration of the respective experiments. The NMR data were processed using Bruker TopSpin 4.3.0.[1]

Powder X-Ray Diffraction

Powder X-Ray Diffraction (PXRD) data were collected using a PANalytical Empyrean diffractometer in a reflection (Bragg-Brentano) geometry with Cu K_α radiation source, Ni K_β filter and PIXcel1D linear detector. Powder diffractograms were recorded in the 5-50° 2θ range with a step size of 0.01303°. Data collection was controlled with X'Pert Data Collector Software.[2]

Single-Crystal X-Ray Diffraction

Single-Crystal X-Ray Diffraction (SCXRD) experiments were run on a Rigaku MiniLab II diffractometer, equipped with a Mo source (λ = 0.71 Å) and Oxford 800 cryostream. Reflections were integrated using the CrysAlias Pro software (v43).[3] The structures were solved by intrinsic phasing and a full matrix least-squares refinement was carried out using all data in Olex2-1.5.[4] Non-hydrogen atoms were refined anisotropically, while hydrogen atoms were added in calculated positions. The crystallographic data for compounds (**1**), (**2**), (**2'**) and (**3**) are shown in Table S1. CIFs have been deposited to the Cambridge Crystallographic Data Centre (CCDC) with deposition numbers 2497061–2497064.

UV-VIS Spectroscopy

Solution UV-VIS spectra were obtained on a Agilent Cary 100 UV-Vis spectrophotometer equipped with a diffuse reflectance accessory. A single baseline scan from 260-900 nm was performed on a 0.1 cm quartz cuvette containing the sample solvent. Sample and baseline data acquisition was performed at a 1 nm resolution set to a 'Medium' scan speed.

Vibrational Spectroscopy

Infrared spectra were obtained on an Agilent Cary 630 FTIR ZnSe engine instrument equipped with a single-bounce diamond ATR sampling accessory, a standard globar source, and a DLaTGS detector.

Differential Scanning Calorimetry

DSC experiments were performed on a TA Instruments Q10 model. The DSC was calibrated at the melting point of the indium metal (156.6 °C). All DSC samples were hermetically sealed in aluminum pans prior to analysis. All samples were heated to 400 °C with a ramp rate of 10 °C min^{-1}, using air as the purge gas. The melting points were measured at the peak of the endothermic process.

Atomic Force Microscopy

AFM data were obtained from a Veeco Dimension 3100 tool, using NanoScope Software. A NuNano AC mode silicon probe was used ("Scout 350 RAl", 42 N/m, 350 kHz). The data was collected in tapping mode, in air, with a scan rate of approximately 0.5 Hz. Scan size and resolution for each acquisition was 25 × 25 μm at 512 × 512 pixels. Raw data was processed and interpreted using WSxM.[5] Standard practice was to flatten the data and remove lines as necessary for clarity. Statistical data was obtained using the statistical quantities tool in Gwyddion.[6]

Scanning Electron Microscopy

Scanning electron microscopy (SEM) measurements were performed using a Tescan VegaII XMU microscope. Prior to imaging, samples were sputter-coated with a thin conductive layer (< 10 nm) of gold (99.99%) using a Quorum Q150T ES sample preparation system to minimize charging effects and improve image quality. The coating was applied uniformly to ensure consistent conductivity across the crystal surface. SEM imaging was conducted under high-vacuum conditions with secondary electron detection to capture surface morphology and fracture features with high resolution.

Commercial Reagents

$Cd(NO_3)_2 \cdot 4H_2O$ and triethylamine (reagent grade) were obtained from Fisher Scientific. 2-hydroxybenzoic acid (2-ohbz) and 4-hydroxybenzoic acid (4-ohbz) was obtained from TCI America.

Starting Materials

(E)-4-(1-naphthylvinylpyridine) (4-nvp) was synthesized according to the procedure outlined by Marczenko *et. al*.[7]

Synthetic Procedure

Synthesis of $Cd_2(4\text{-ohbz})_4(4\text{-nvp})_4$ (**1**): 4-nvp (0.043 g, 0.185 mmol) was dissolved in 2.5 mL of methanol and carefully layered on top of a 1.0 mL deionized water solution of $Cd(NO_3)_2 \cdot 4H_2O$ (0.029 g, 0.093 mmol) in a 4-dram vial. A solution of 4-ohbz (0.026 g, 0.188 mmol) dissolved in 2.5 mL of 95% ethanol was prepared and neutralized with NEt_3 (26.2 μL, 0.187 mmol). This solution was carefully layered on top of the previous two layers to form a three-layer system. The vial was wrapped in tin foil to reduce light exposure and put into a low light environment to grow yellow crystals over 4 days. ^{1}H-

NMR (DMSO-d_6, 300 MHz): δ 9.83 (4H, s, OH), 8.58 (2H, d, *J* = 6 Hz), 8.45 (4H, d, *J* = 9 Hz), 8.37 (4H, d, *J* = 16 Hz), 7.96 (12H, m), 7.77 (16H, m), 7.60 (12H, m), 7.31 (4H, d, *J* = 16 Hz).

Synthesis of Cd_2(2-ohbz)$_4$(4-nvp)$_4$ (**2**): A solution of 4-nvp (0.048 g, 0.207 mmol) dissolved in 2.5 mL of methanol was layered carefully on top of a $Cd(NO_3)_2 \cdot 4H_2O$ (0.032 g, 0.103 mmol) solution dissolved in 1 mL of methanol in a 4-dram vial. Finally, a 2-ohbz (0.029 g, 0.209 mmol) solution dissolved in 2.5 mL of methanol and neutralized with NEt_3 (30.0 µL, 0.215 mmol) was subsequently layered. The three-layer solution was wrapped in tin foil to reduce exposure to light and put in a low light environment to grow yellow crystals over a week. The procedure can be replicated by alternatively dissolving $Cd(NO_3)_2 \cdot 4H_2O$ and 2-ohbz in deionized water and 95% ethanol, respectively. (0.035 g, 21% yield). M.P. = 217 – 242 °C. ^{1}H-NMR (DMSO-d_6, 300 MHz): δ 14.17 (4H, s, OH), 8.59 (8H, d, *J* = 6 Hz), 8.46 (4H, d, *J* = 9 Hz), 8.38 (4H, d, *J* = 16 Hz), 8.02-7.91 (12H, m), 7.81-7.72 (12H, m), 7.66-7.53 (12H, m), 7.36-7.22 (8H, m), 6.80-6.68 (8H, m).

Synthesis of Cd_2(2-ohbz)$_4$(rcct-4-pncb)$_2$ (rctt-4-pncb = 1,3-bis(4'pyridyl)-2,4-bis(naphthyl)cyclobutane (**3):** Complex (**2**) was irradiated for 45–60 minutes using a DARKBEAM 10 W, 365 nm lithium-ion battery flashlight (T7 bulb, 200 lumens). ^{1}H-NMR (DMSO-d_6, 300 MHz): δ 13.98 (4H, s, OH), 8.38 (8H, d, *J* = 8 Hz), 8.22 (4H, d, *J* = 8 Hz), 8.02 (4H, d, *J* = 8 Hz), 7.91–7.71 (12H, m), 7.66-7.53 (12H, m), 7.36-7.22 (8H, m), 6.78-6.72)*H, m), 5.56 (4H, dd, *J* = 7 Hz, CH cyclobutane), 4.79 (4H, dd, *J* = 7 Hz, CH cyclobutane).

2 Powder X-ray Diffraction

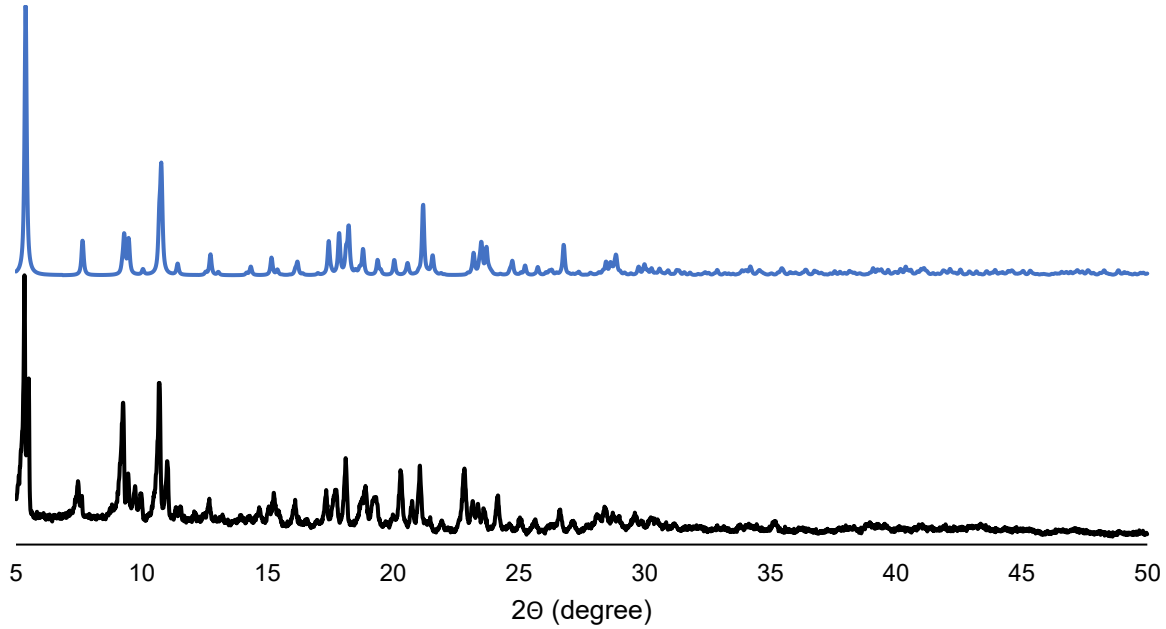

Figure S1. Powder X-ray Diffraction pattern of **1** (experimental, black; calculated, blue) at 293 K.

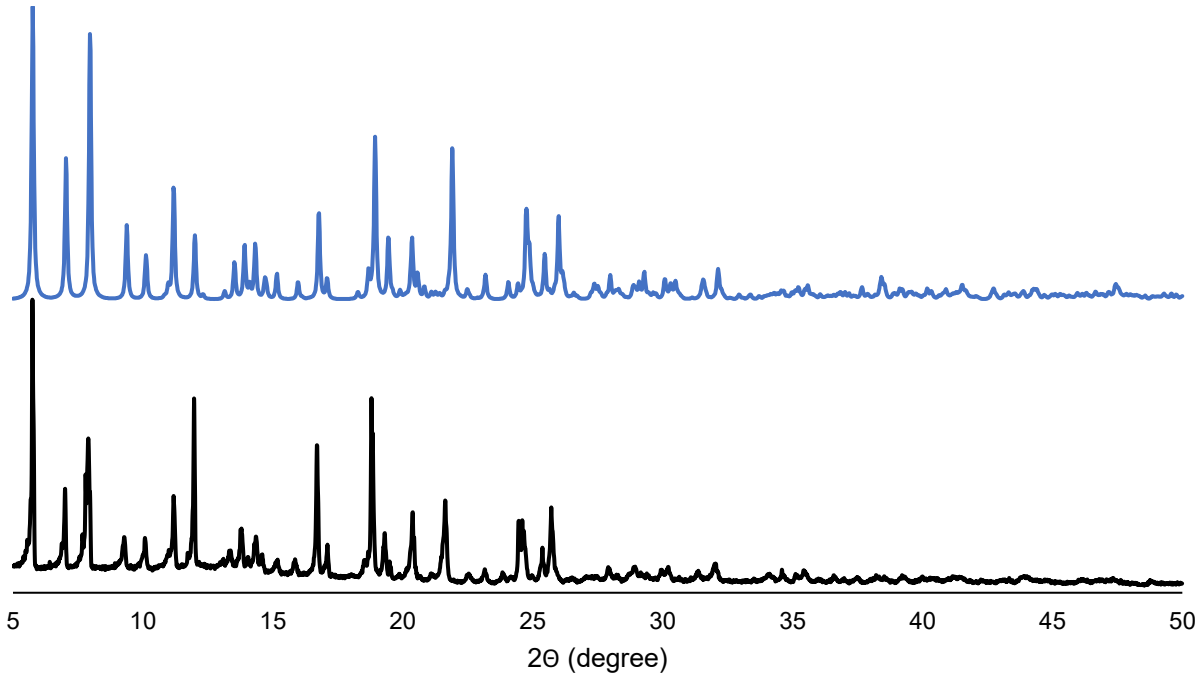

Figure S2. Powder X-ray Diffraction pattern of **2** (experimental, black; calculated, blue) at 293 K.

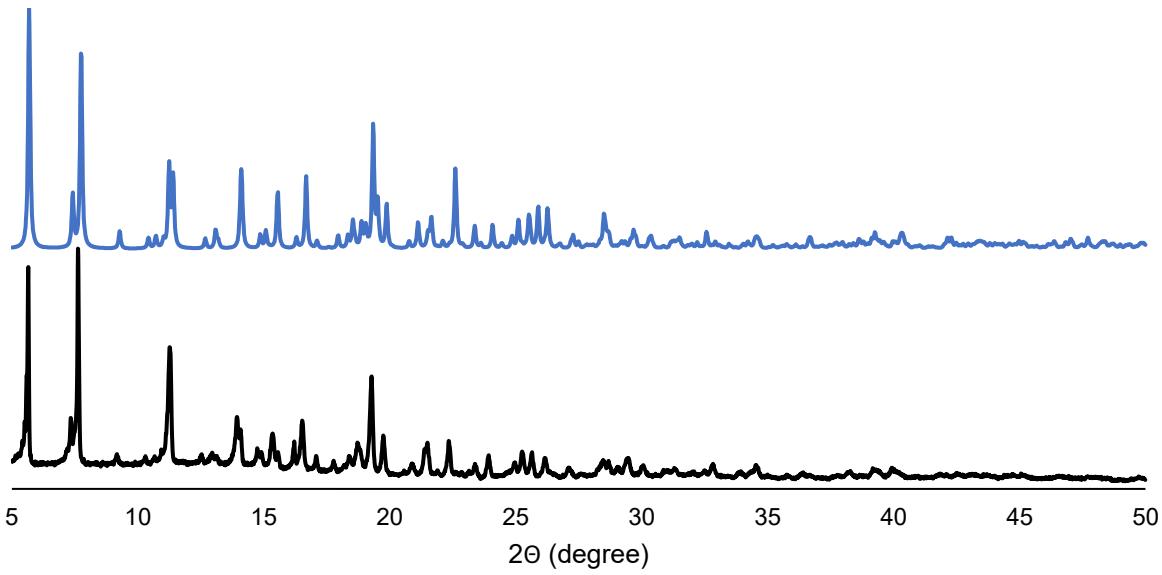

Figure S3. Powder X-ray Diffraction pattern of **3** (experimental, black; calculated, blue) at 293 K.

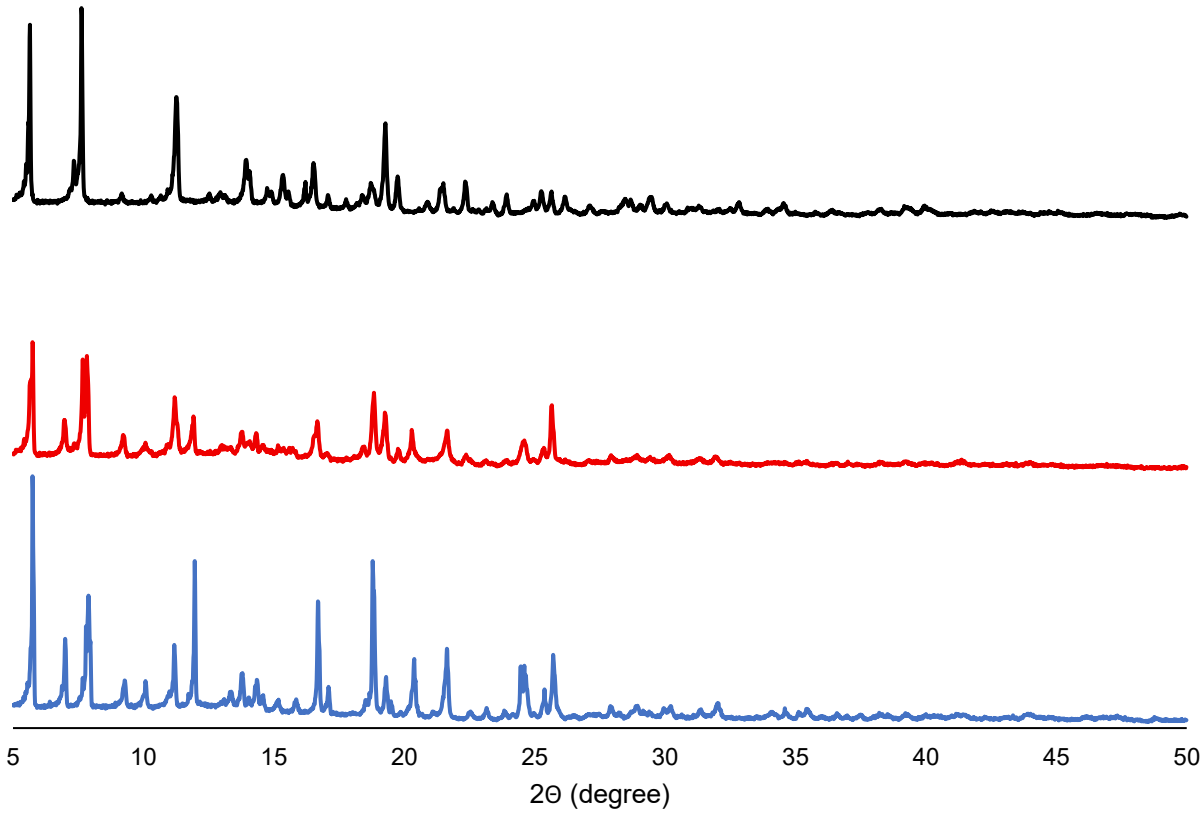

Figure S4. Powder X-ray Diffraction pattern of **2** at 0 min (blue), 3 min (red; **2'**) and 45 min (black; **3**) of UV-radiation at 293 K.

3 Spectroscopy

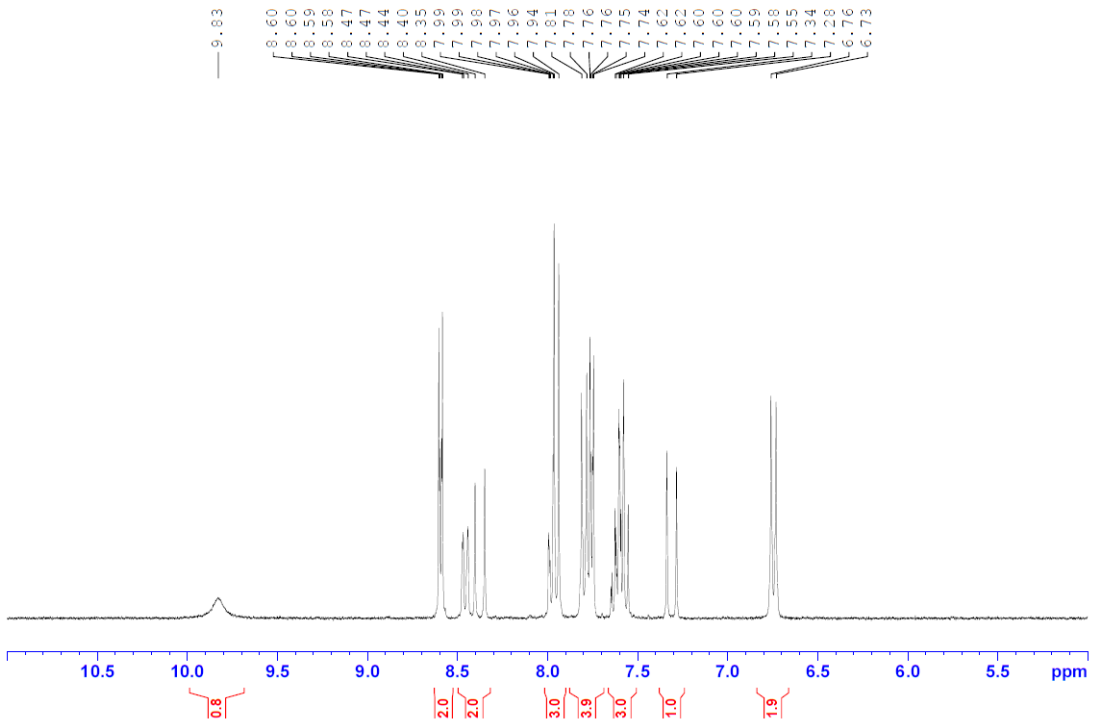

Figure S5. ^{1}H NMR (300 MHz; dimethyl sulfoxide-d_6) of **1**.

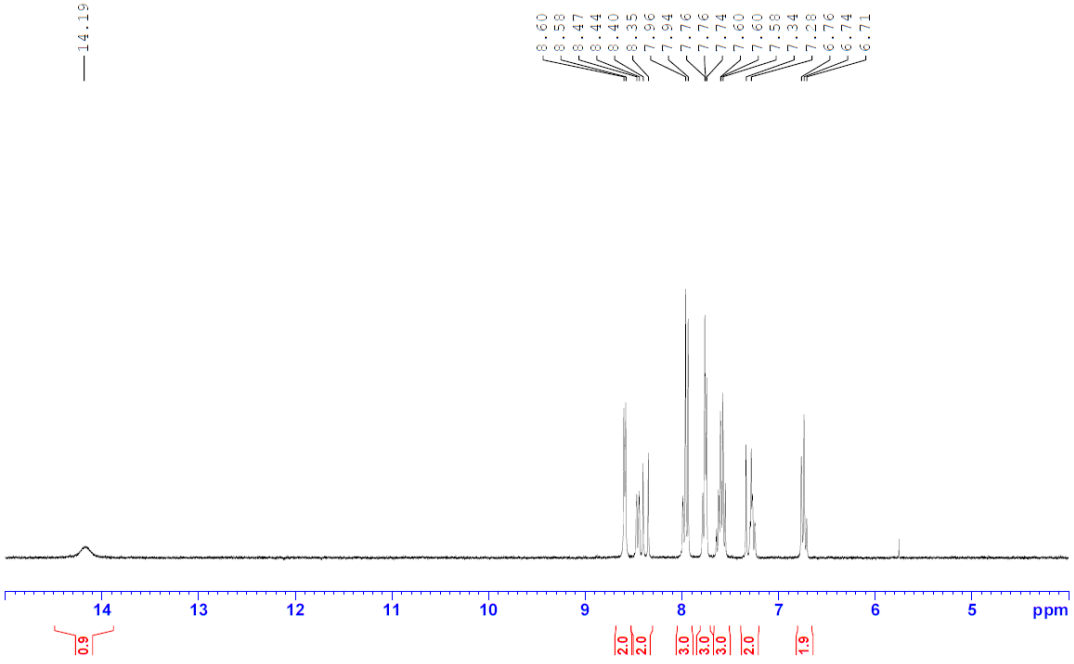

Figure S6. ^{1}H NMR (300 MHz; dimethyl sulfoxide-d_6) of **2**.

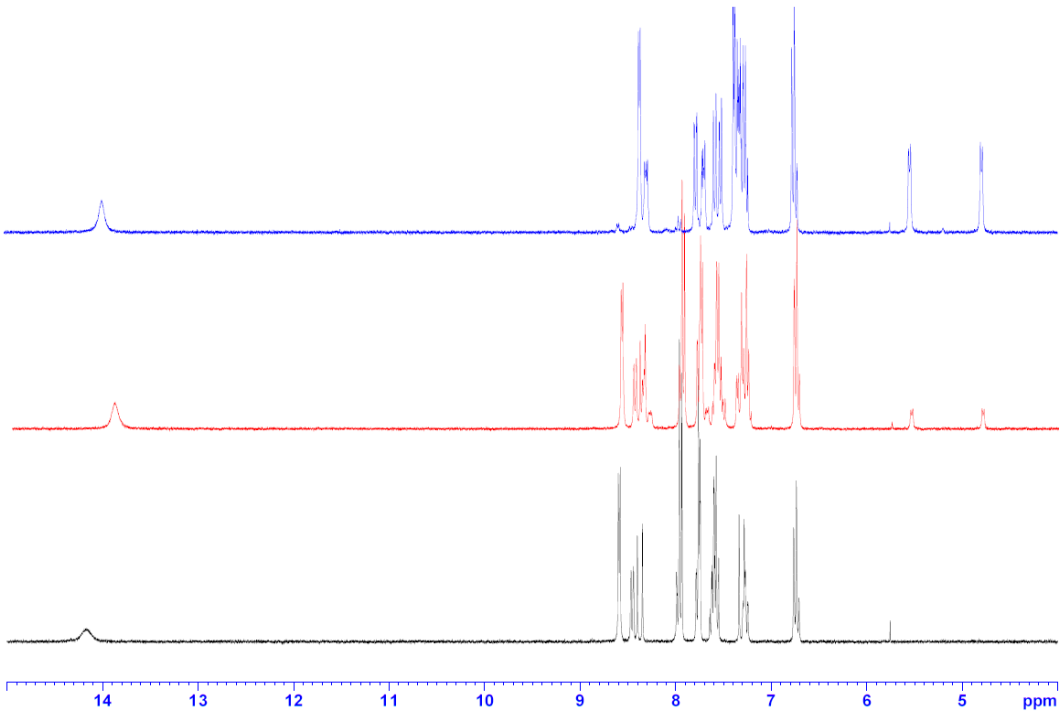

Figure S7. ^{1}H NMR (300 MHz; dimethyl sulfoxide-d_6) of **2** after 0 min (black), 3 min (red), and 45 min (blue) of UV-light irradiation.

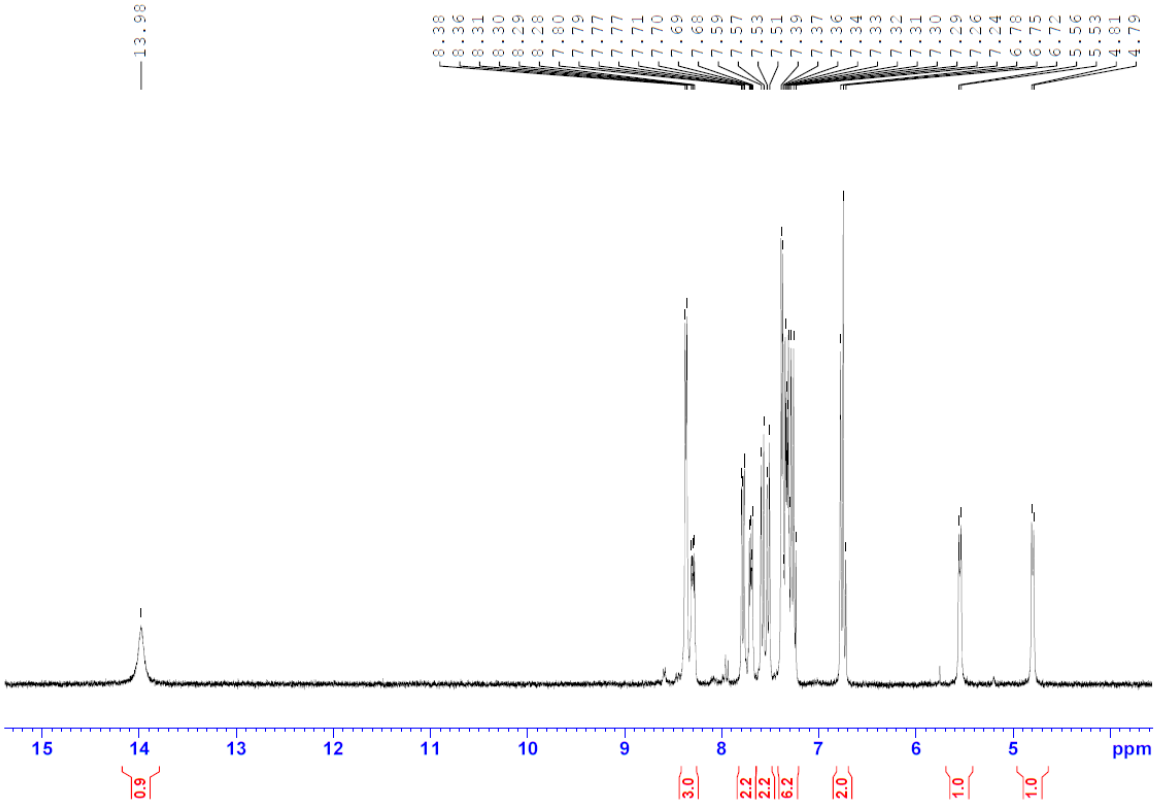

Figure S8. ^{1}H NMR (300 MHz; dimethyl sulfoxide-d_6) of **3**.

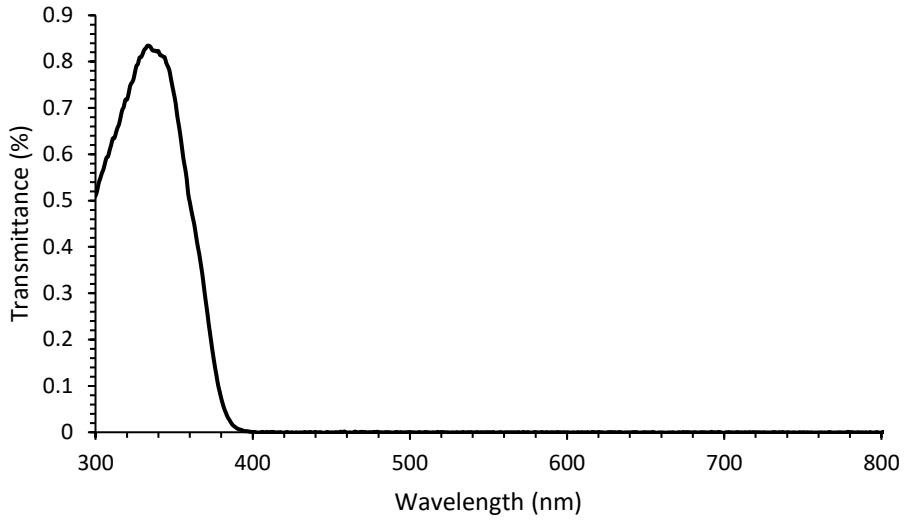

Figure S9. Blank corrected UV-Vis spectrum of a 5.0×10^{-5} M solution of **2** in DMSO (λ_{max} = 340 nm).

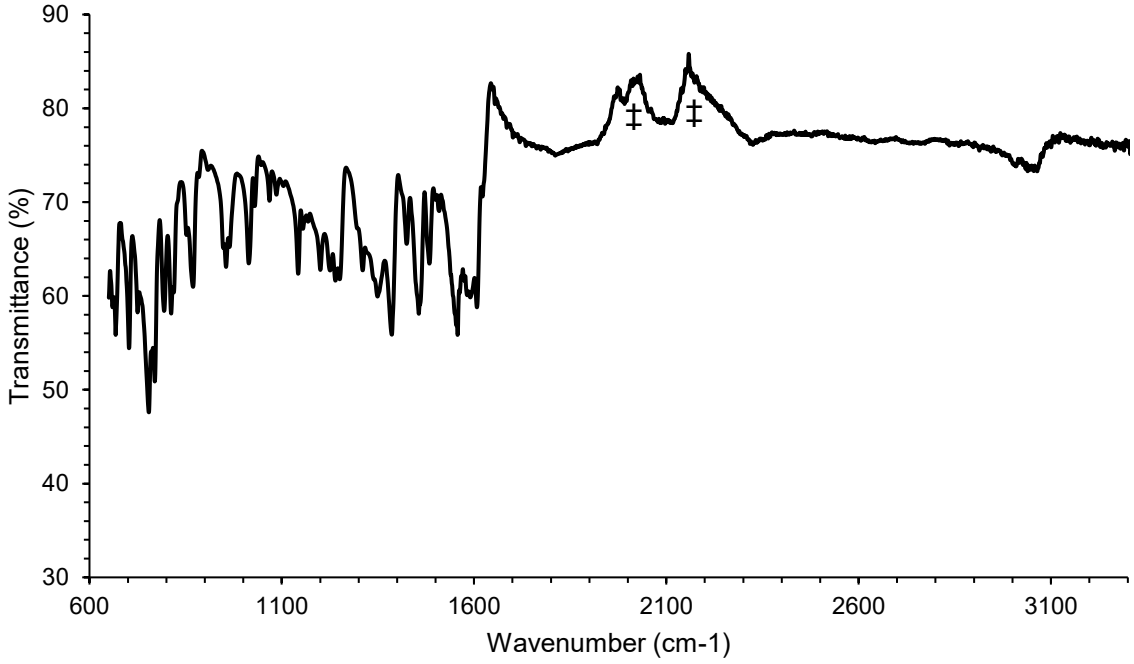

Figure S10. FTIR spectrum of **2**, acquired from 64 scans at 2 cm^{-1} resolution for both background and sample measurements. A Happ Genzel apodization and Mertz phase correction was applied. The symbol ‡ indicates artifacts from the diamond ATR crystal.[8]

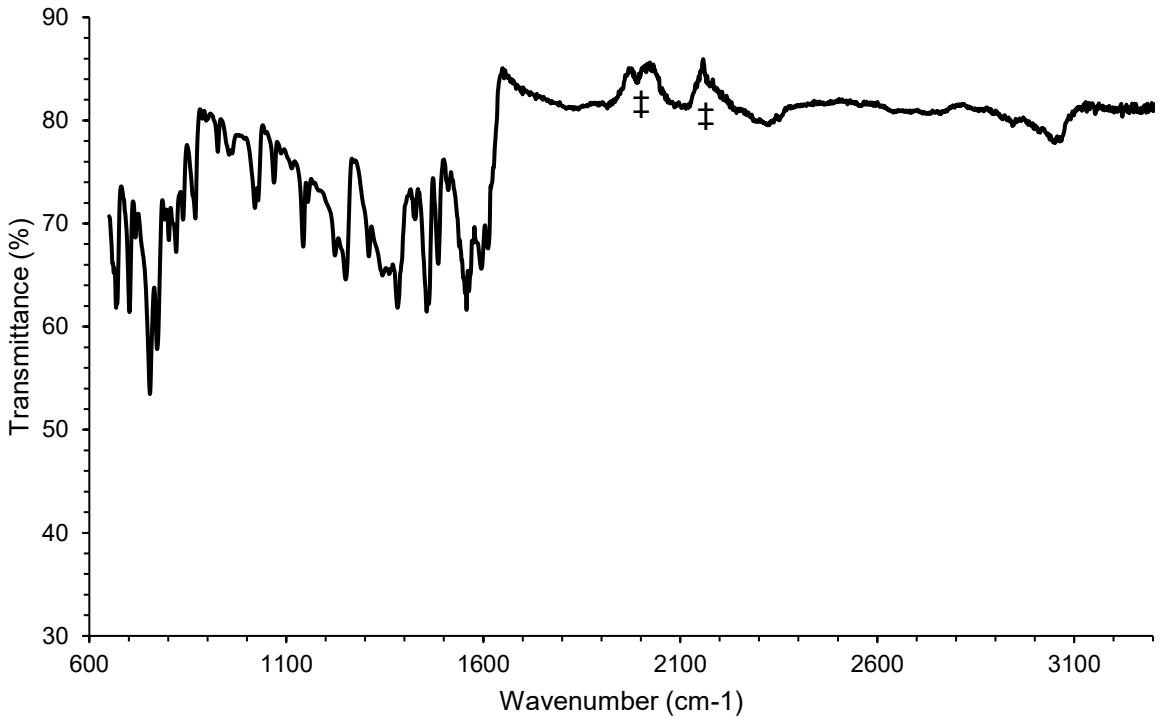

Figure S11. FTIR spectrum of **3**, acquired from 64 scans at 2 cm^{-1} resolution for both background and sample measurements. A Happ Genzel apodization and Mertz phase correction was applied. The symbol ‡ indicates artifacts from the diamond ATR crystal.[8]

4 Calorimetry

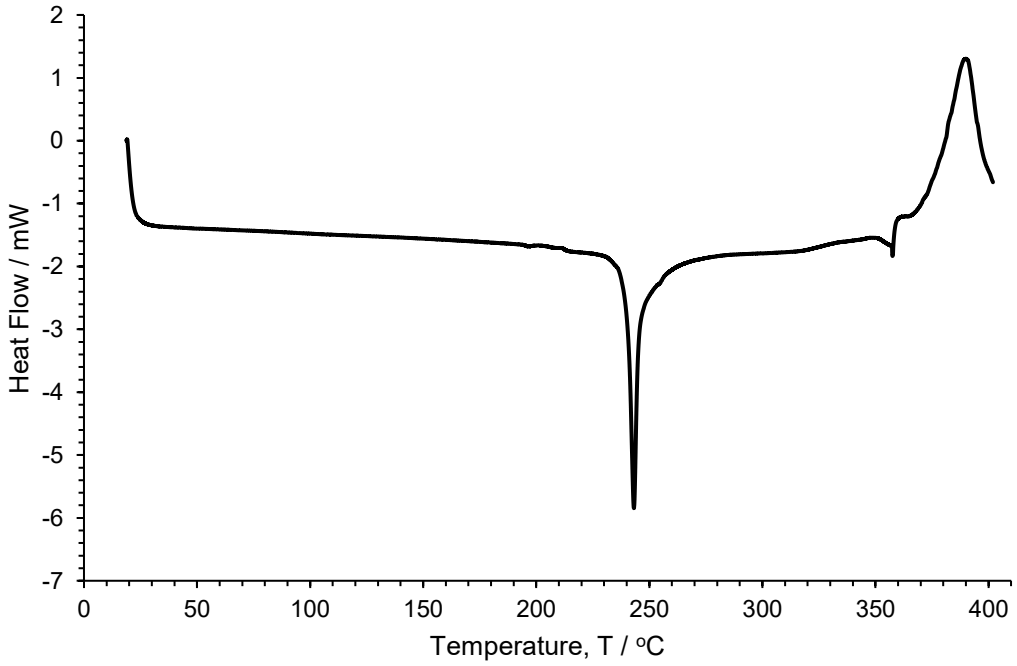

Figure S13. DSC thermogram of **2**. A sample size of 1.5 mg and ramp rate of 5.00 °C /min from room temperature (20.05 °C) to 400.00 °C was used.

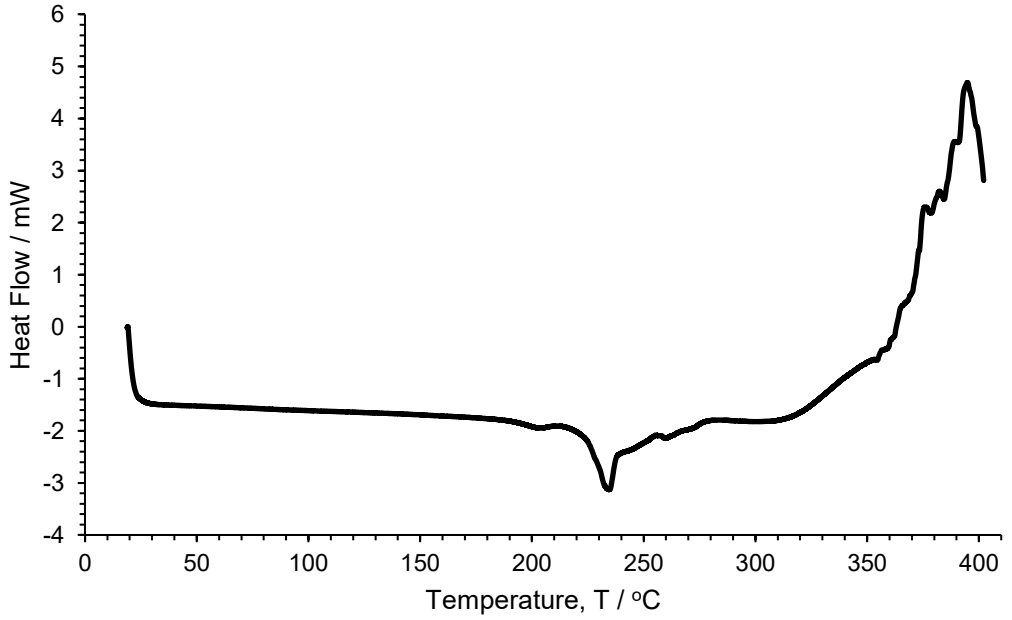

Figure S14. DSC thermogram of **2** after 3 min of UV-radiation (i.e. **2'**). A sample size of 1.8 mg and ramp rate of 5.00 °C /min from room temperature (20.05 °C) to 400.00 °C was used.

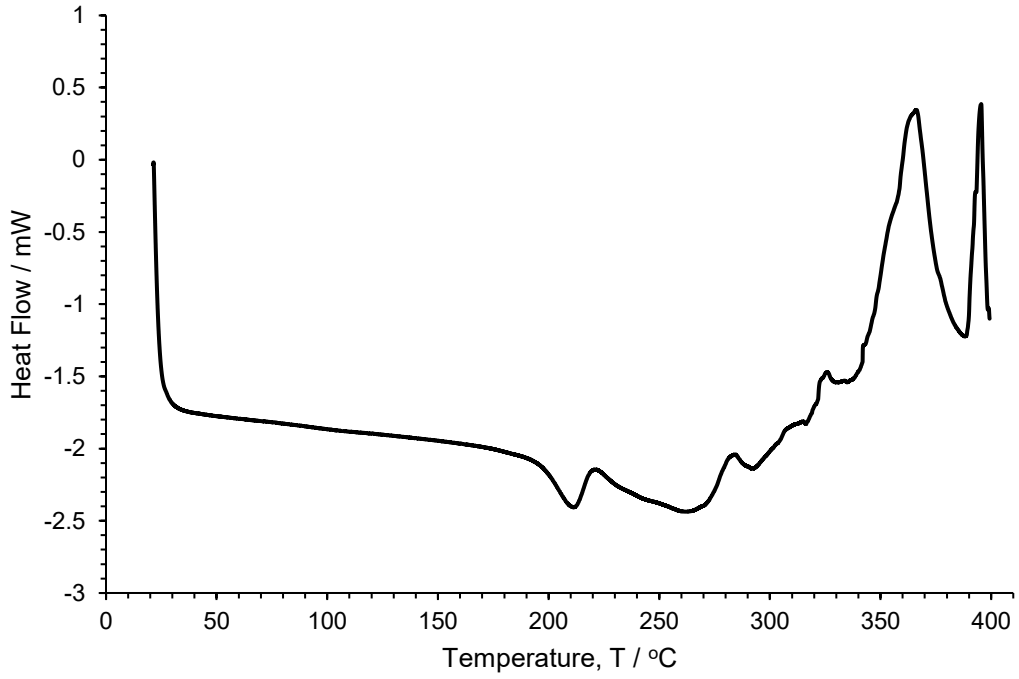

Figure S15. DSC thermogram of 2 after 1 hour of UV-radiation (**i.e.** 3). A sample size of 1.7 mg and ramp rate of 5.00 °C /min from room temperature (20.05 °C) to 400.00 °C was used.

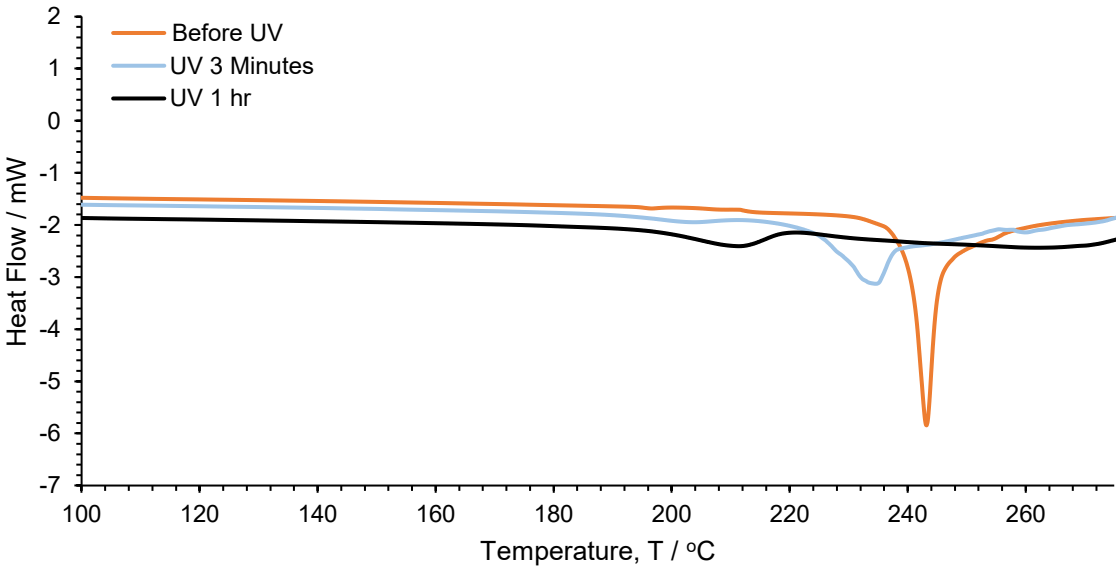

Figure S16. Stacked DSC thermogram of 2 after 0 min, 3 min, and 1 hour of UV-radiation.

5 X-ray Crystallography

Table S1. Crystal data and refinement parameters for **(1), (2), (2'),** and **(3)**. The same crystal was used to monitor the progression from 2 → 2' → 3.

	(1)	(2)	(2')	(3)
Identification code	Cd_FormII_115K	VPT-i-82-115K	VPT-i-82-365nm10W-3min-115K	VPT-i-82-365nm10W-45min-115K
Empirical formula	$C_{96}H_{72}Cd_2N_4O_{12}$	$C_{96}H_{71.24}Cd_2N_4O_{12}$	$C_{96}H_{71.8}Cd_2N_4O_{12}$	$C_{48}H_{36}CdN_2O_6$
Formula weight	1698.37	1697.61	1698.17	849.19
Temperature/K	140.15	115.00(10)	115.00(10)	115.00(10)
Crystal system	monoclinic	triclinic	triclinic	triclinic
Space group	$P2_1/c$	P-1	P-1	P-1
a/Å	16.4115(6)	9.7798(4)	9.8283(3)	9.8104(2)
b/Å	10.4173(4)	13.3815(5)	12.9535(8)	12.9237(4)
c/Å	23.1085(7)	15.7776(6)	16.3591(9)	16.4017(4)
α/°	90	76.532(3)	71.857(5)	71.569(3)
β/°	91.640(3)	88.255(3)	89.889(4)	89.871(2)
γ/°	90	74.683(3)	76.841(4)	76.937(2)
Volume/Å^3	3949.1(2)	1935.62(13)	1921.82(18)	1916.40(9)
Z	2	1	1	2
ρ_{calc}g/cm^3	1.428	1.456	1.467	1.472
μ/mm^{-1}	0.607	0.619	0.623	0.625
F(000)	1736.0	867.0	868	868.0
Crystal size/mm^3	0.345 × 0.212 × 0.088	0.41 × 0.18 × 0.08	0.36 × 0.14 × 0.1	0.35 × 0.13 × 0.11
Radiation/Å	MoKα (λ = 0.71073)	Mo Kα (λ = 0.71073)	Mo Kα (λ = 0.71073)	Mo Kα (λ = 0.71073)
2Θ range for data collection/°	4.632 to 62.014	4.32 to 52.83	4.784 to 52.868	4.274 to 52.842
Index ranges	-23 ≤ h ≤ 23, -14 ≤ k ≤ 14, -33 ≤ l ≤ 32	-12 ≤ h ≤ 12, -16 ≤ k ≤ 16, -19 ≤ l ≤ 19	-12 ≤ h ≤ 12, -15 ≤ k ≤ 16, -20 ≤ l ≤ 20	-12 ≤ h ≤ 12, -16 ≤ k ≤ 16, -20 ≤ l ≤ 20
Reflections collected	44601	31694	31068	44615
Independent reflections	11961 [R_{int} = 0.0691, R_{sigma} = 0.1077]	7859 [R_{int} = 0.0417, R_{sigma} = 0.0396]	7788 [R_{int} = 0.0648, R_{sigma} = 0.0842]	7774 [R_{int} = 0.0416, R_{sigma} = 0.0351]
Data/restraints/parameters	11961/3/516	7859/53/581	7788/620/608	7774/551/582
Goodness-of-fit on F^2	1.008	1.017	1.078	1.036
Final R indexes [I>=2σ (I)][a,b]	R_1 = 0.0560, wR_2 = 0.1074	R_1 = 0.0321, wR_2 = 0.0721	R_1 = 0.0611, wR_2 = 0.1249	R_1 = 0.0297, wR_2 = 0.0629
Final R indexes [all data][a,b]	R_1 = 0.1151, wR_2 = 0.1255	R_1 = 0.0428, wR_2 = 0.0757	R_1 = 0.0947, wR_2 = 0.1347	R_1 = 0.0405, wR_2 = 0.0664
Largest diff. peak/hole / e Å^{-3}	1.64/-0.94	0.73/-0.71	1.60/-1.16	0.97/-0.84

$$^{a}R_1 = \frac{\Sigma|F_o - F_c|}{\Sigma|F_o|} \qquad ^{b}wR_2 = \sqrt{\frac{\Sigma w(F_o - F_c)^2}{\Sigma w(F_o)^2}}$$

Table S2. Summary of crystallographic parameters of **2**, before (0 min), during (**2'**, 3 min; "Cracks"), and after irradiation (**3**, 45 min; "Healed") at 115 K.

Parameter	2 0 min	2' 3 min ("Cracked")	3 45 min ("Healed")	Δ(2→2′) % ±σ	Δ(2′→3) % ±σ	Δ(0→45 min) % ±σ
a (Å)	9.7798(4)	9.8283(3)	9.8104(2)	+0.496 ± 0.0051	−0.182 ± 0.0037	+0.313 ± 0.0046
b (Å)	13.3815(5)	12.9535(8)	12.9237(4)	−3.198 ± 0.0070	−0.230 ± 0.0069	−3.421 ± 0.0047
c (Å)	15.7776(6)	16.3591(9)	16.4017(4)	+3.686 ± 0.0069	+0.260 ± 0.0060	+3.956 ± 0.0047
α (°)	76.532(3)	71.857(5)	71.569(3)	−6.109 ± 0.0075	−0.401 ± 0.0081	−6.485 ± 0.0054
β (°)	88.255(3)	89.889(4)	89.871(2)	+1.851 ± 0.0057	−0.020 ± 0.0050	+1.831 ± 0.0041
γ (°)	74.683(3)	76.841(4)	76.937(2)	+2.890 ± 0.0068	+0.125 ± 0.0058	+3.018 ± 0.0049
Volume (Å³)	1935.62(14)	1921.82(18)	1916.40(9)	−0.713 ± 0.0117	−0.282 ± 0.0104	−0.993 ± 0.0085

$$\Delta \boldsymbol{X}\ (\%) = \frac{(\boldsymbol{X_2} - \boldsymbol{X_1})}{|\boldsymbol{X_1}|} \times \mathbf{100}$$

Equation S1. Percent change was calculated according to the above equation, where X_1 is value 1 and X_2 is value 2, and ΔX is the calculated change value in percent.

$$\Delta\sigma = \left(\frac{X_2}{X_1}\right)\sqrt{\left(\frac{\sigma_1}{X_1}\right)^2 + \left(\frac{\sigma_2}{X_2}\right)^2} \times 100$$

Equation S2. Formula used for propagation of uncertainty in **Table S4**.

Uncertainties in the percent change values were determined by propagation of errors from the standard deviations of the refined crystallographic parameters. Percent changes were calculated using equation s1, where x_1 and x_2 are the refined values of each parameter before and after irradiation, respectively. The corresponding uncertainties were obtained using equation S2. All uncertainties are reported at the one-sigma (1σ) confidence level and are rounded to two significant digits. Percent change values are presented to three decimal places to reflect the propagated precision and to prevent rounding of small uncertainties to zero. The same method was applied for both stepwise (0 → 3 min, 3 → 45 min) and cumulative (0 → 45 min) changes. Because the number of formula units per unit cell (Z) remains constant across all structures, the propagated uncertainty for Δ(V/Z) is identical to that for Δ(V).

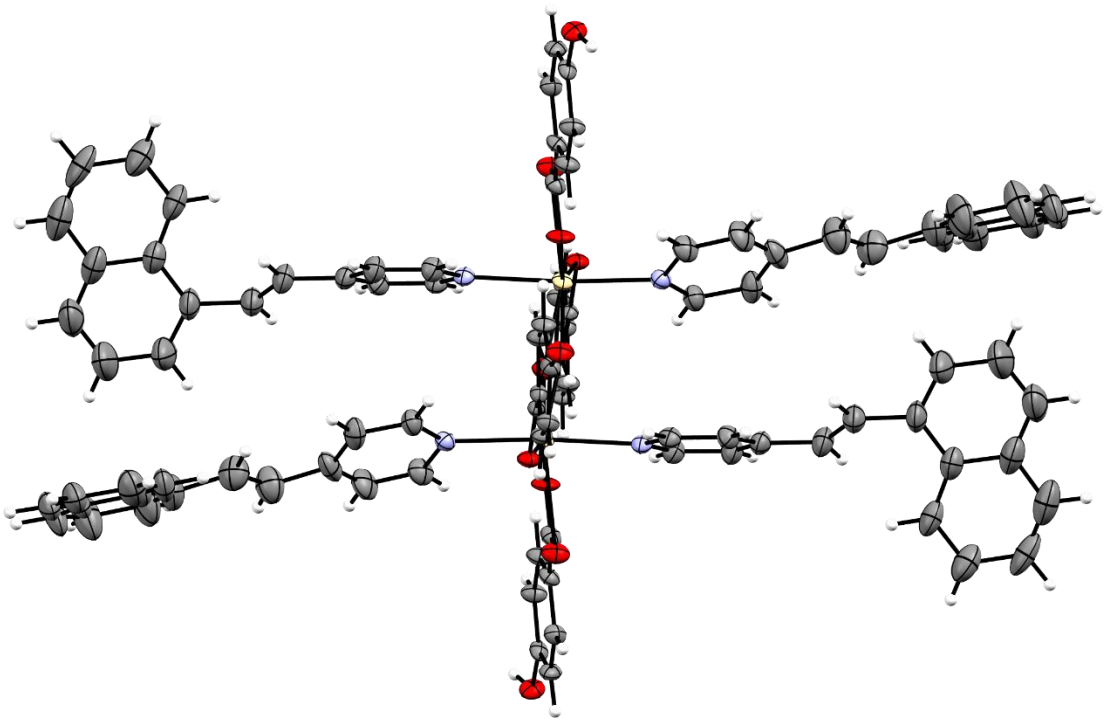

Figure S17. Single crystal x-ray structure of **1**. The molecular unit is shown and thermal ellipsoids are drawn at the 50% probability level.

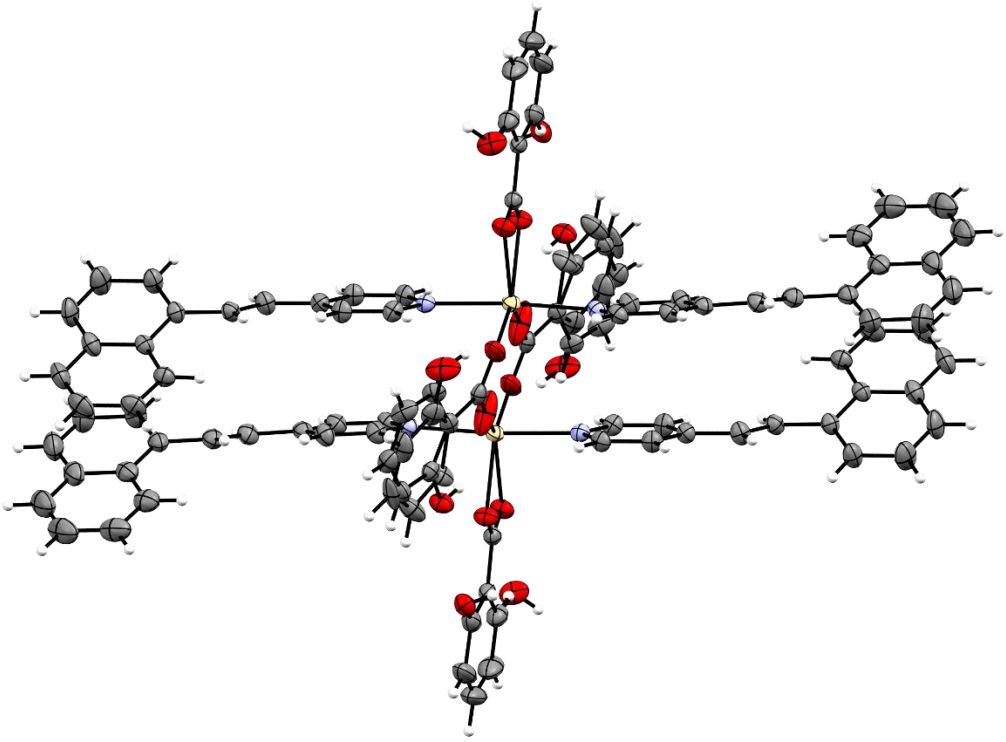

Figure S18. Single crystal x-ray structure of **2**. The molecular unit is shown and thermal ellipsoids are drawn at the 50% probability level.

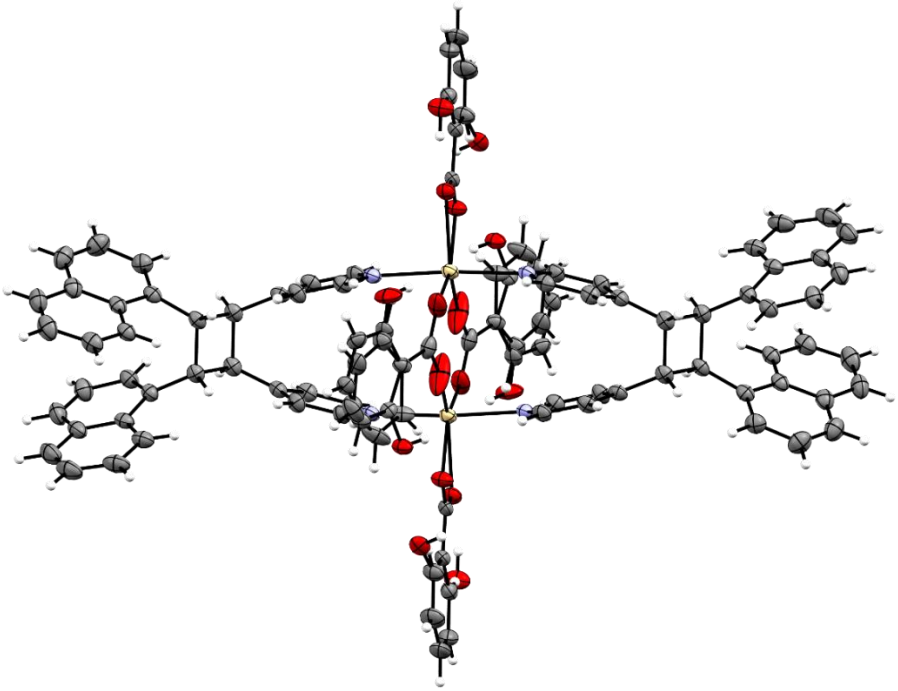

Figure S19. Single crystal x-ray structure of **3**. The molecular unit is shown and thermal ellipsoids are drawn at the 50% probability level.

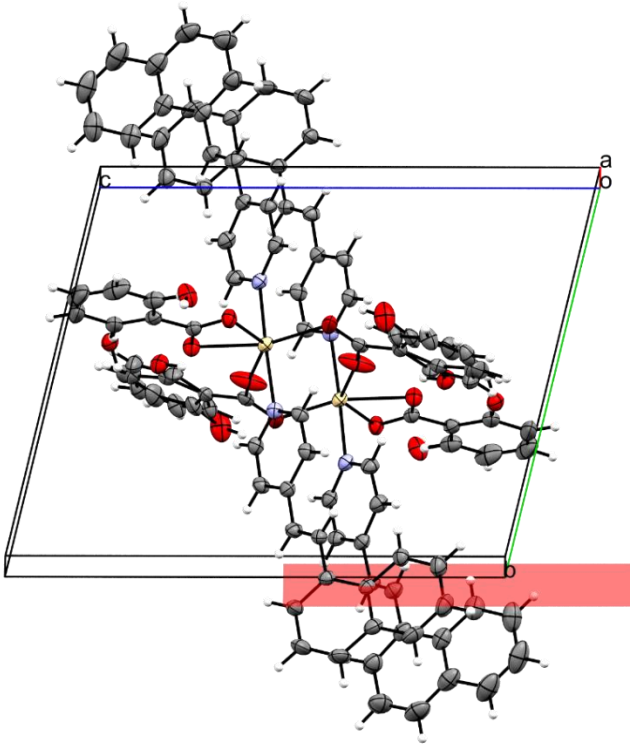

Figure S20. Single crystal x-ray structure of **3**. The molecular unit is shown and thermal ellipsoids are drawn at the 50% probability level.

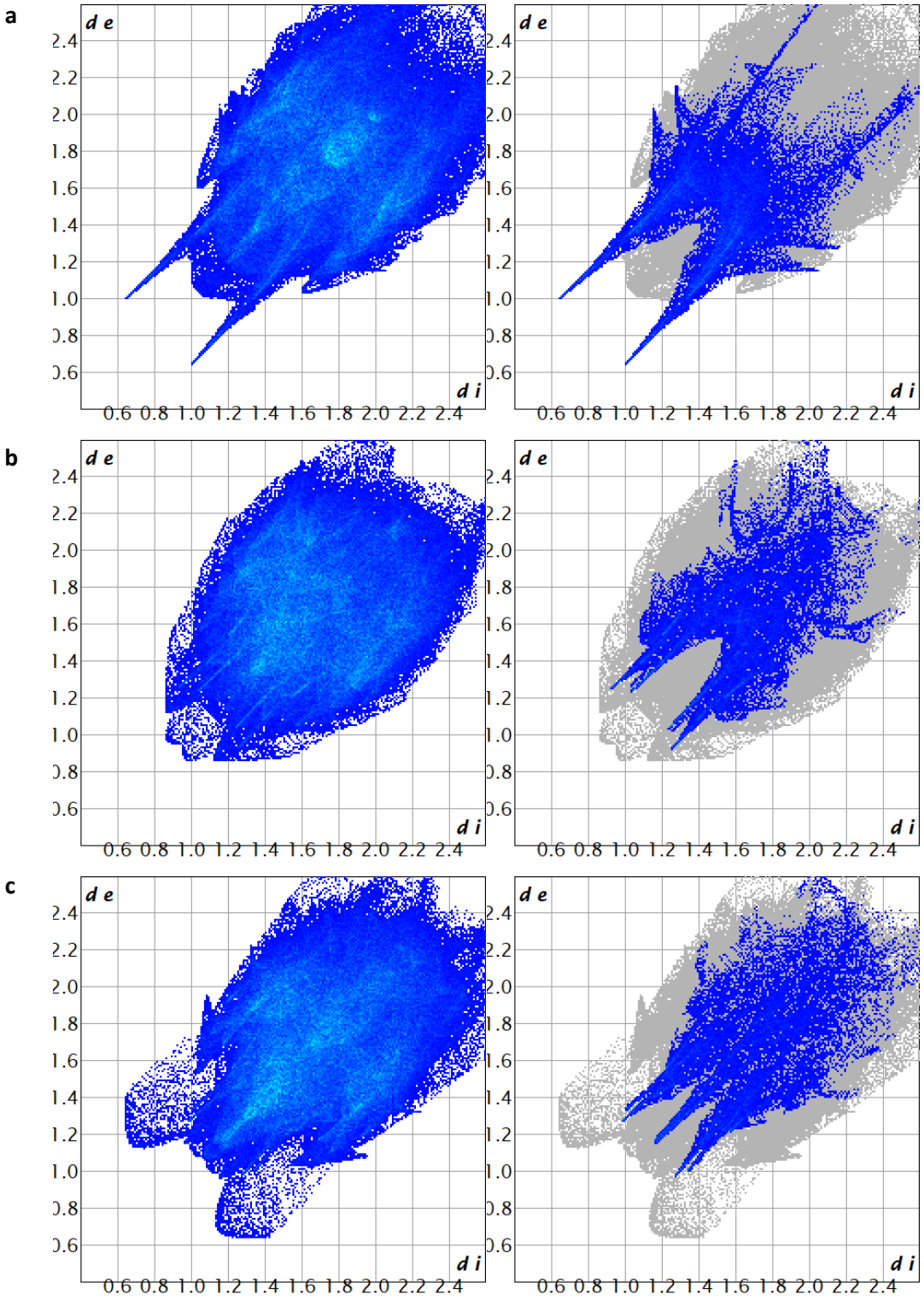

Figure S21. Two-dimensional fingerprint plot for compounds **1**, **2**, and **3** showing all interactions (left) and O···H interactions (right). The d_i and d_e values are the closest internal and external distances (in Å) from given points on the Hirshfeld surface.

6 Microscopy

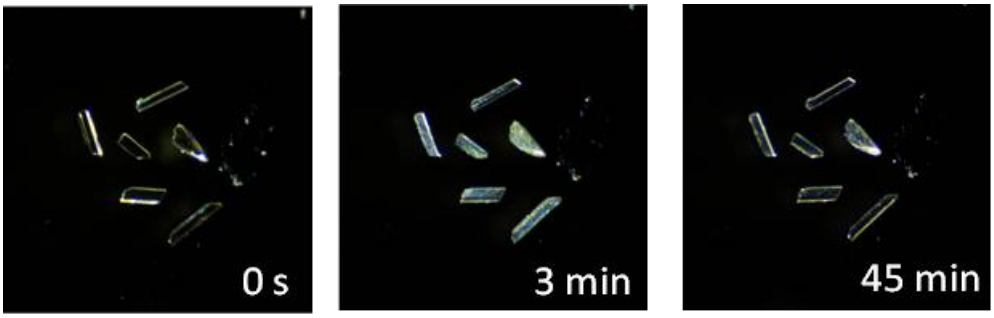

Figure S22. A series of photographs taken on Zeiss Stereomicroscope Stemi 305 under darkfield.

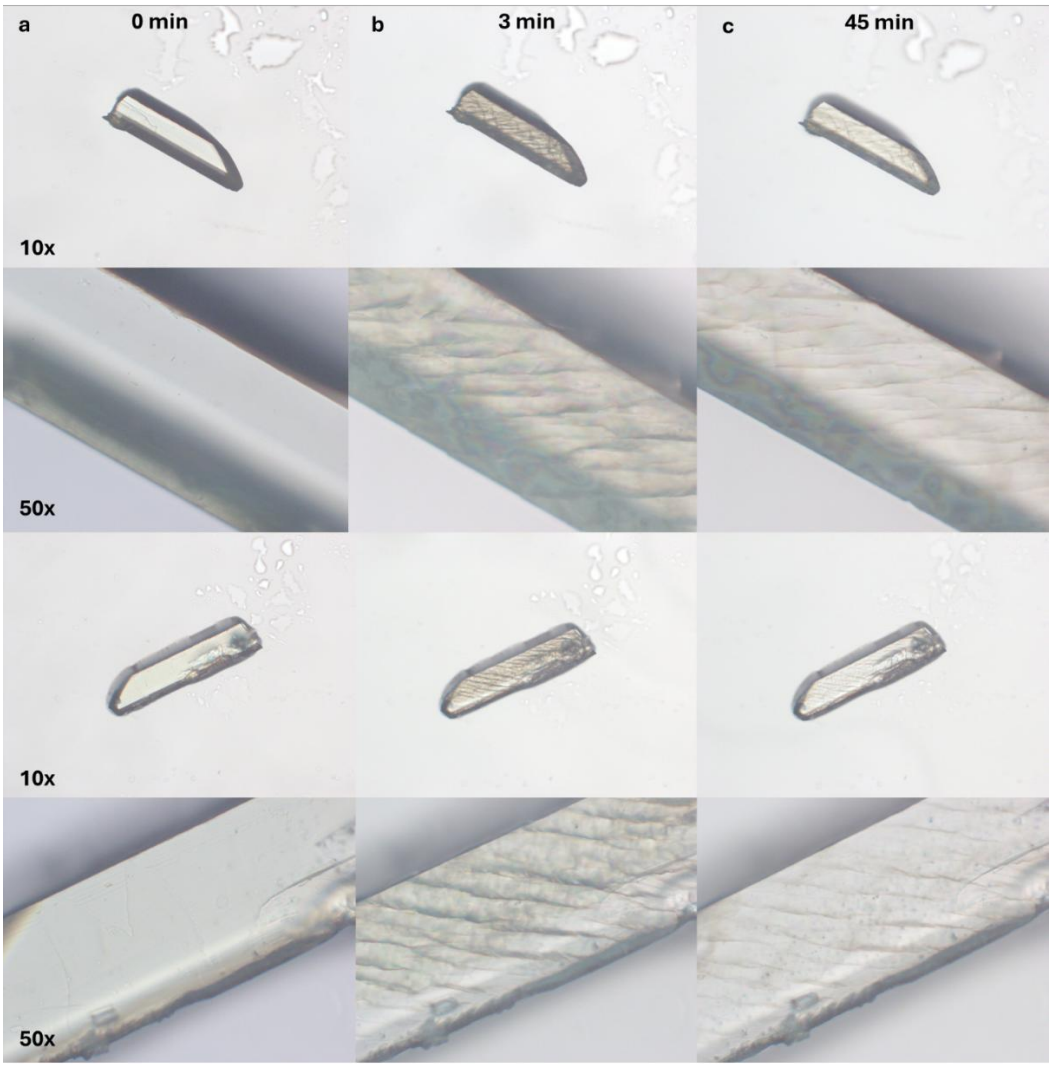

Figure S23. A series of photographs taken on Mitutoyo Japan Ultraplan FS110 equipped with a Lumenera Infinity 2 camera.

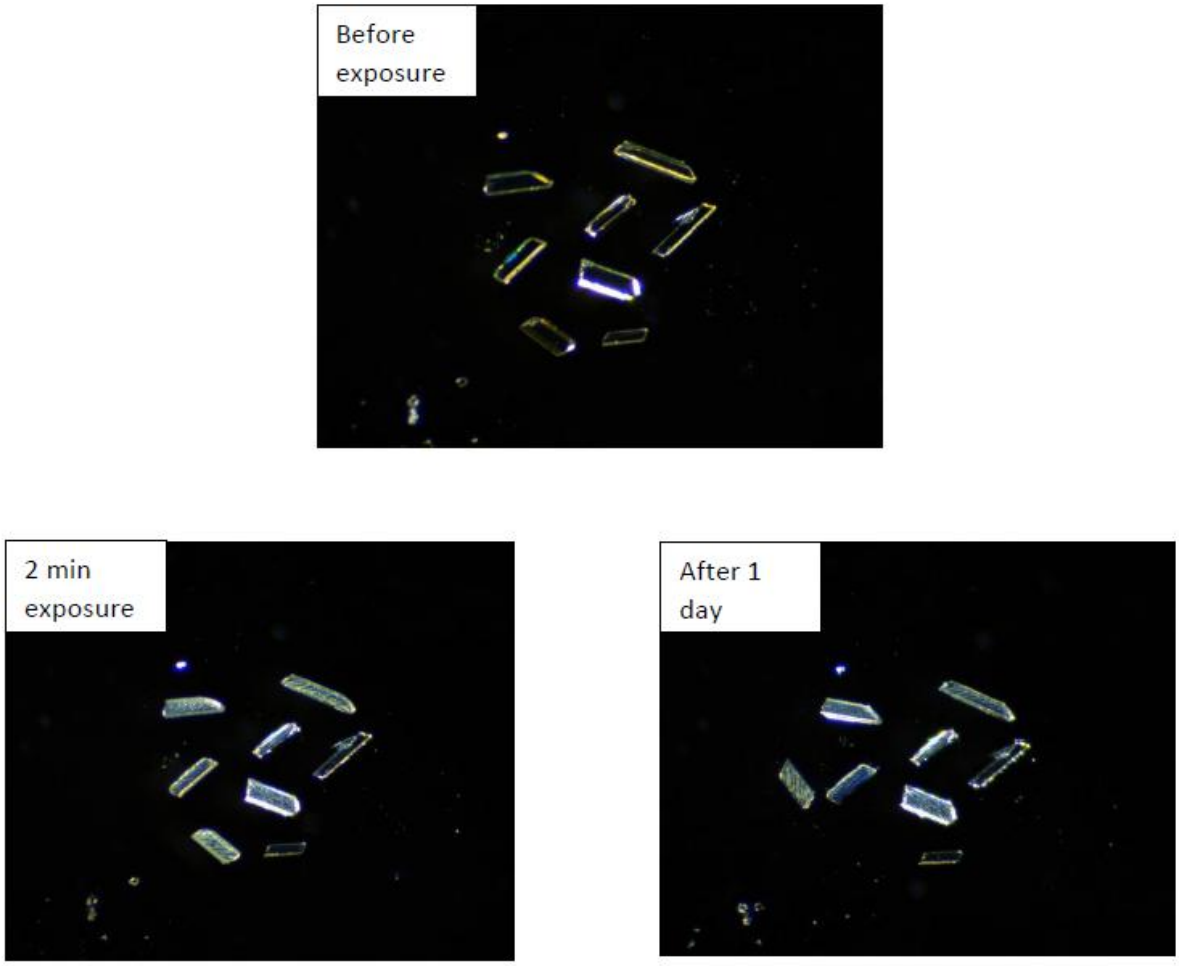

Figure S24. Optical images of crystals of **2** collected after (a) 2 min of UV irradiation and (b) following a 30 min rest period in the absence of UV light taken on Zeiss Stereomicroscope Stemi 305 under darkfield.

.

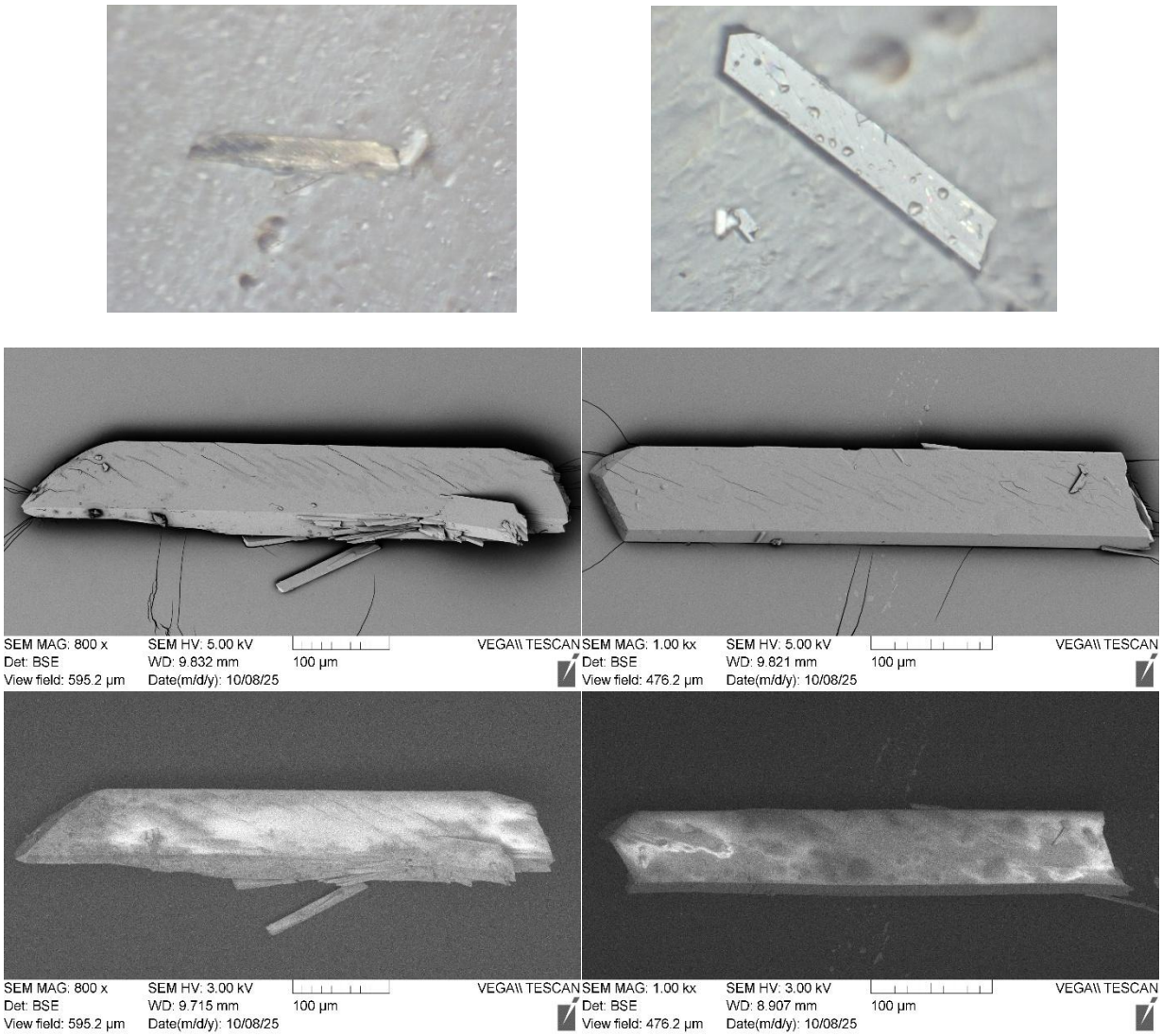

Figure S25. Optical (top) and SEM images (below) of fractured crystals of Cd_2(2-ohbz)$_4$(4-nvp)$_4$. The optical micrograph images show the as-prepared crystals prior to coating.

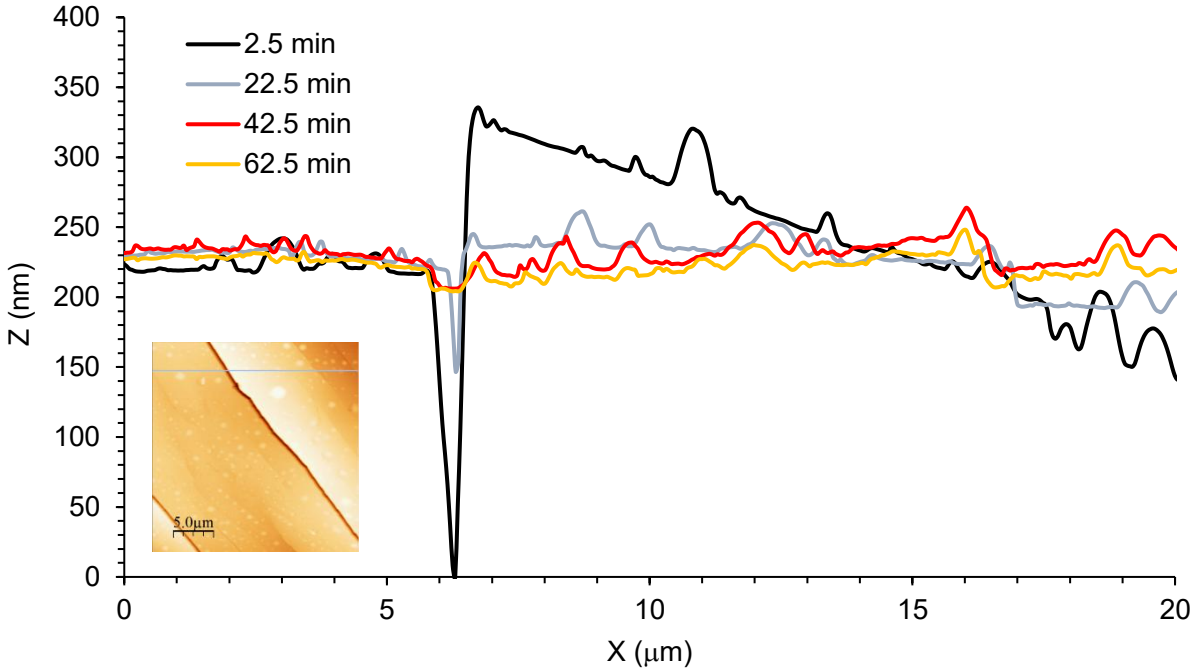

Figure S26. AFM line profile analysis of $Cd_2(4\text{-nvp})_4(2\text{-ohbz})_4$ crystals following UV irradiation for 2.5-, 22.5-, 42.5-, and 62.5-min. Plots of height (z, nm) versus lateral distance (x, μm) were obtained from the line indicated in the representative AFM image (25 μm × 25 μm scan).

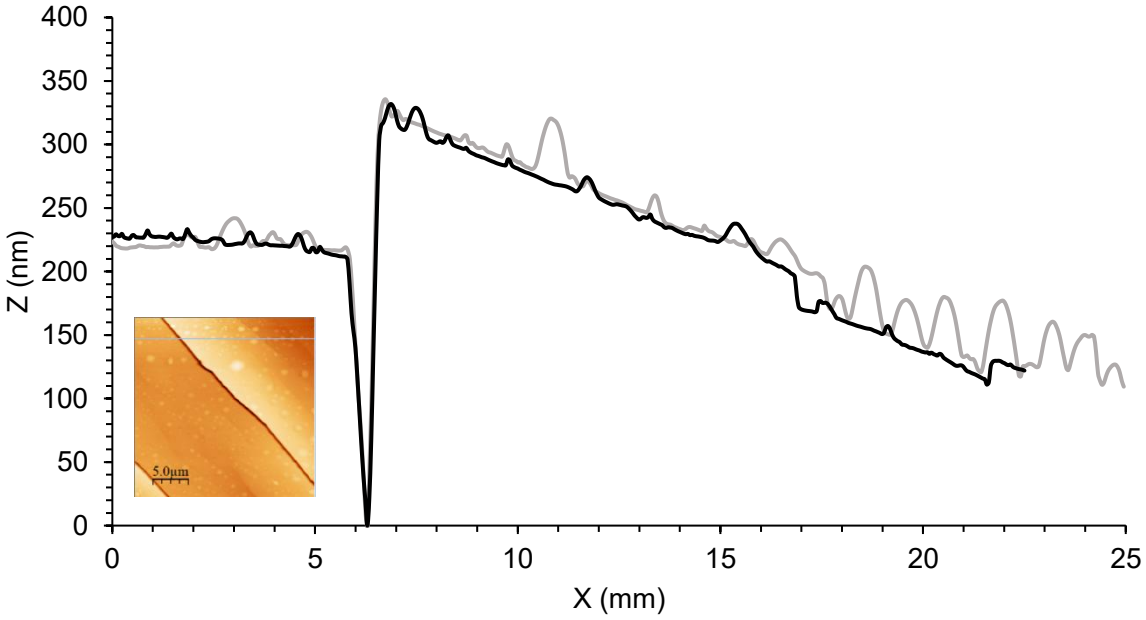

Figure S27. AFM line profile analysis of $Cd_2(4\text{-nvp})_4(2\text{-ohbz})_4$ crystals following UV irradiation for 2.5 min (grey)and a rest period of 50 min (black). Plots of height (z, nm) versus lateral distance (x, μm) were obtained from the line indicated in the representative AFM image (25 μm × 25 μm scan).

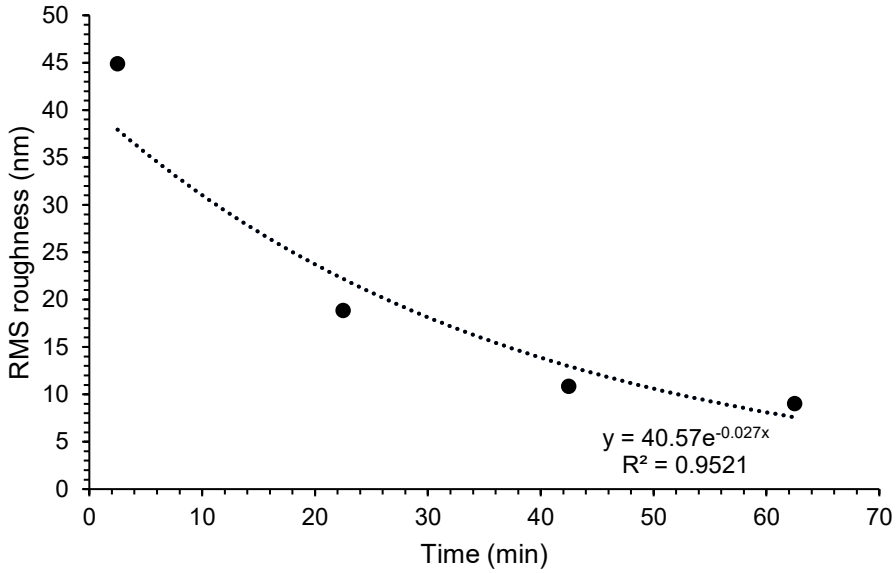

Figure S28. Time-dependent decay of RMS surface roughness (S_q) measured by AFM. The data were fitted to an exponential decay function $y = y_o e^{-kx}$.

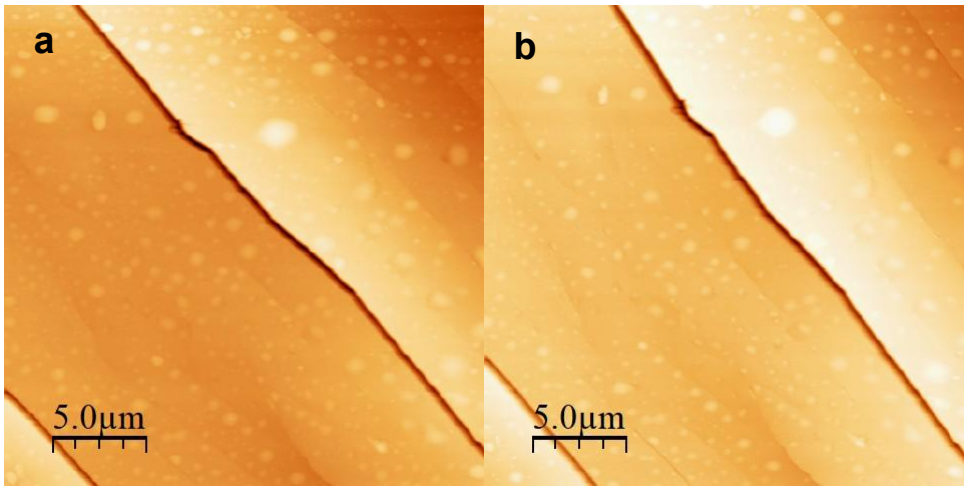

Figure S29. Topographic atomic force microscopy (AFM) images of the crystal surface of (**2**) collected after (a) 2.5 min of UV irradiation and (b) following a 50 min rest period in the absence of UV light.

Table S3. Statistical surface parameters obtained from AFM analysis of a single crystal of $Cd_2(4\text{-nvp})_4(2\text{-ohbz})_4$ following sequential UV irradiation and rest periods. AFM scans were collected after an initial 2.5 min UV exposure, after a 50 min rest in ambient light, and after three additional UV irradiation intervals of 20 min each (22.5-, 42.5-, and 62.5-min total exposure).

	2.5 min	**2.5 min** (rest)	**22.5 min**	**42.5 min**	**62.5 min**
Average value (nm)	0	0	0	0	0
RMS roughness (S_q; (nm)	52.1514	44.8881	18.8448	10.8498	9.01935
RMS (grain-wise; nm)	52.1514	44.8881	18.8448	10.8498	9.01935
Mean roughness (S_a; nm)	38.7888	31.6673	13.4431	7.5926	6.35289
Skew (S_{sk})	-0.30071	-0.68068	-0.58632	0.809425	0.515816
Excess kurtosis	2.13654	3.57195	4.54622	6.25525	4.69789
Minimum (nm)	-305.323	-313.694	-193.865	-139.599	-88.123
Maximum (nm)	212.261	135.588	84.576	82.099	66.135
Median (nm)	-9.978	-5.824	-0.391	-0.04	0.102
Maximum peak height (S_p; nm)	212.261	135.588	84.576	82.099	66.135
Maximum pit depth (S_v; nm)	305.323	313.694	193.865	139.599	88.123
Maximum height (S_z; nm)	517.584	449.282	278.441	221.697	154.258
Surface area (mm^2)	635.118	632.832	628.812	626.888	625.924
Surface slope (S_{dq}; mm^2)	0.20839	0.178222	0.125324	0.0803222	0.05583
Volume (pm^3)	898.67	-345.332	-301.787	21.2046	260.829
Variation (mm^2)	51.5928	43.1005	33.9305	37.5159	25.2749
Inclination θ (deg)	0.33	0.31	0.07	0.01	0
Inclination φ (deg)	144.36	151.26	137.08	188.9	192.04
Scan line discrepancy	0.045317	0.039015	0.136059	0.214277	0.157814

7 References

1. Bruker Biospin. *TopSpin Software*, Version 4.0.7; Bruker Biospin GmbH: Karlsruhe, Germany, 2017.
2. PANalytical. *X'Pert Data Collector Software*, Version 5.3.0.62; PANalytical B.V.: Almelo, Netherlands, 2015.
3. Agilent. *CrysAlis PRO*; Agilent Technologies Ltd.: Yarnton, Oxfordshire, England, 2014.
4. Dolomanov, O. V.; Bourhis, L. J.; Gildea, R. J.; Howard, J. A. K.; Puschmann, H. *J. Appl. Crystallogr.* **2009**, *42*, 339–341.
5. Horcas, I.; Fernández, R.; Gómez-Rodríguez, J. M.; Colchero, J.; Gómez-Herrero, J.; Baró, A. M. *Rev. Sci. Instrum.* **2007**, *78*, 013705.
6. Nečas, D.; Klapetek, P. *Cent. Eur. J. Phys.* **2012**, *10* (1), 181–188.
7. Moffat, J. G. D.; Pham-Tran, V. N. P.; Marczenko, K. M. *Can. J. Chem.* **2024**, *102*, 794–801.
8. Yan, B.; Jia, X.; Sun, S.; Zhou, Z.; Fang, C.; Chen, N.; Li, Y.; Li, Y.; Ma, H. *Int. J. Refract. Met. Hard Mater.* **2015**, *48*, 56–60.